RESEARCH ARTICLE

NANO · MICRO small
www.small-journal.com

An Adhesive Bioink toward Biofabrication under Wet Conditions

Wanlu Li, Mian Wang, Shiwei Wang, Xiaoping Wang, Alan Avila, Xiao Kuang, Xuan Mu, Carlos Ezio Garciamendez, Zewei Jiang, Jennifer Manríquez, Guosheng Tang, Jie Guo, Luis Santiago Mille, Juan Antonio Robledo, Di Wang, Feng Cheng, Hongbin Li, Regina Sanchez Flores, Zhibo Zhao, Clément Delavaux, Zixuan Wang, Arturo López, Sili Yi, Cuiping Zhou, Ameyalli Gómez, Carl Schuurmans, Guo-Yuan Yang, Yongting Wang, Xingcai Zhang, Ximu Zhang,* and Yu Shrike Zhang**

Three-dimensional (3D) bioprinting is driving significant innovations in biomedicine over recent years. Under certain scenarios such as in intraoperative bioprinting, the bioinks used should exhibit not only cyto/biocompatibility but also adhesiveness in wet conditions. Herein, an adhesive bioink composed of gelatin methacryloyl, gelatin, methacrylated hyaluronic acid, and skin secretion of *Andrias davidianus* is designed. The bioink exhibits favorable cohesion to allow faithful extrusion bioprinting in wet conditions, while simultaneously showing good adhesion to a variety of surfaces of different chemical properties, possibly achieved through the diverse bonds presented in the bioink formulation. As such, this bioink is able to fabricate sophisticated planar and volumetric constructs using extrusion bioprinting, where the dexterity is further enhanced using ergonomic handheld bioprinters to realize in situ bioprinting. In vitro experiments reveal that cells maintain high viability; further in vivo studies demonstrate good integration and immediate injury sealing. The characteristics of the bioink indicate its potential widespread utility in extrusion bioprinting and will likely broaden the applications of bioprinting toward situations such as in situ dressing and minimally invasive tissue regeneration.

1. Introduction

Bioprinting has emerged as a pivotal approach used toward fabricating scaffolds containing living cells for biomedical applications. For instance, regeneration of bone,[1] cartilage,[2] skin,[3] liver,[4] and nerve tissues,[5] as well as tissue modeling for disease investigations and drug screening, have been achieved with three-dimensional (3D) bioprinting.[6,7] One methodology of bioprinting is intraoperative bioprinting (IOB), where a bioink is in real-time patterned on a living object for tissue repair during a surgical procedure.[8–10] Direct bioprinting onto the injury region provides an effective means of fitting the formed graft precisely to the wound geometry. Localized control over the deposition of biomaterials, cells, cytokines, and/or other components mimics the natural heterogeneity, further

W. Li, M. Wang, S. Wang, A. Avila, X. Kuang, X. Mu, C. E. Garciamendez, Z. Jiang, J. Manríquez, G. Tang, J. Guo, L. S. Mille, J. A. Robledo, D. Wang, F. Cheng, H. Li, R. S. Flores, Z. Zhao, C. Delavaux, Z. Wang, A. López, S. Yi, C. Zhou, A. Gómez, C. Schuurmans
Division of Engineering in Medicine
Department of Medicine
Brigham and Women's Hospital
Harvard Medical School
Cambridge, MA 02139, USA

W. Li, G.-Y. Yang, Y. Wang
School of Biomedical Engineering and Med-X Research Institute
Shanghai Jiao Tong University
Shanghai 20030, P. R. China

The ORCID identification number(s) for the author(s) of this article can be found under https://doi.org/10.1002/smll.202205078.

DOI: 10.1002/smll.202205078

S. Wang
National Center for International Joint Research of Micro-Nano Molding Technology
School of Mechanics & Safety Engineering
Zhengzhou University
Zhengzhou 450001, P. R. China

X. Wang, X. Zhang, Y. S. Zhang
Chongqing Key Laboratory of Oral Disease and Biomedical Sciences & Chongqing Municipal Key Laboratory of Oral Biomedical Engineering of Higher Education & Stomatological Hospital of Chongqing Medical University
Chongqing 401174, P. R. China
E-mail: zhangximu@hospital.cqmu.edu.cn; yszhang@research.bwh.harvard.edu

A. Avila, J. Manríquez, A. López, A. Gómez
Biotechnology Program
Tecnológico de Monterrey
Monterrey, NL 64849, México

promoting tissue remodeling.[11] In addition, compared to tissues implanted after in vitro bioprinting, IOB minimizes the risks of contamination and disturbance originating from sample transferring or manual interventions.[11] As such, IOB is an emerging and promising technique increasingly applied to tissue repairs especially for the regeneration of cutaneous tissues such as the bone, cartilage, and skin.[12]

As an effective IOB tool, handheld bioprinters based on extrusion methods have been innovated to reconstruct the injured structures with morphological and physiological relevancies to the native tissues under the surgeons' controls.[13,14] For example, a handheld 3D bioprinter (Biopen) based on the coaxial extrusion method was innovated, and a type of bioink containing gelatin methacryloyl (GelMA), methacrylated hyaluronic acid (HAMA), and mesenchymal stem cells (MSCs) was applied to fabricating scaffolds in situ for cartilage regeneration.[15] An inevitable obstacle would be maintaining the position of the bioprinted scaffolds due to the wet operating conditions (wounds featuring wet surfaces or surroundings), which would result in insufficient immediate adhesion between the deposited bioscaffolds and the host tissues. In this aforementioned study,[15] a layer of commercial fibrin glue was additionally sprayed on top of the bioprinted scaffold to tackle the adhesive problems. However, this fibrin glue might lead to operational complexity and hinder the integration of implanted bioscaffolds, especially for clinical translational applications.

Considering the fact that IOB is directly processed into a defect site that is oftentimes moisturized or entirely immersed in body fluids, particular criteria need to be met for IOB bioinks beyond the general bioink requirements. Under moisturized surgical conditions, the hydration layer of body fluid generally prohibits the tight contact and stable adhesion between tissue surfaces and deposited bioinks, creating obstacles in terms of adhesion.[16–18] When applying IOB to surgical settings, ideal bioinks are expected to be conveniently patterned, rapidly form high-fidelity architectures in the moist environment, and firmly adhere to the underlying wound areas with retained shape integrity. Guaranteeing graft/host adhesion in IOB could maintain the correct positions and structural integrities after bioprinting, and further improve the tissue regeneration with the aid of the bioprinted constructs possessing bionic architectures and biomimetic cell distributions. Nevertheless, bioinks that can achieve adequate adhesion between bioprinted constructs and host tissue surfaces, in particular wounded surfaces that are oftentimes wet, have hardly been investigated so far especially in the context of in situ bioprinting.[19,20]

Here, we report a method for bioprinting in wet conditions with our developed adhesive bioink formulation composed of GelMA, gelatin, HAMA, and skin secretion of *Andrias davidianus* (SSAD). The diagram of our bioprinting strategy on diverse surfaces is shown in **Figure 1**a,b. It is believed that the favorable adhesion capability of our unique bioink is mediated by the $\pi-\pi$ electron/cation$-\pi$ interactions, hydrophobic interactions, as well as hydrogen bonds between the bioink and various substrates of diverse surface chemical properties. These substrates include not only biological tissues but also common surfaces used for bioprinting, such as tissue culture-treated petri dish, plastic (pristine polystyrene), glass, and silicone polymer, suggesting the versatility of the bioink for general bioprinting applications as well as the IOB methodology. The bioink formulation is tested with different components for cohesiveness, adhesiveness, and bioprinting fidelity. Using this adhesive bioink, a variety of patterns is bioprinted in wet conditions with multi-material, multi-layer, and/or multi-interface capacities at optimized bioprinting parameters. Moreover, the cyto/biocompatibility of the (bio)printed constructs is evaluated both in vitro and in vivo. Finally, to achieve manipulation dexterity, a handheld bioprinter based on the extrusion approach is subsequently designed and demonstrated.

2. Results and Discussion

SSAD is a newly discovered biomaterial containing a number of polypeptides and proteins that can be involved in diverse physiological functions.[21] Our previous studies have indicated that the rich composition of tyrosine, phenylalanine, and other amino acids makes it an effective bioinspired adhesive for wound healing.[22–24] However, the SSAD powder by itself is hardly soluble in water and exhibits rapid aggregation and further gelation when contacting water, largely resulting from the unique nature of the positively charged surface and hydrophobic domains of SSAD.[23] To improve desired distribution of SSAD in the bioink, we selected HAMA possessing a highly negative zeta-potential to disperse SSAD, thus giving rise to excellent suspension stability of SSAD.[25] HAMA is derived from hyaluronic acid abundantly available in connective, epithelial, and neuronal tissues of the human body.[26] We synthesized different molecular weights (M_w) of HAMA, ranging from 10 to 1000 kDa. The distribution of SSAD improved with the M_w of HAMA increasing under the same concentration (Figure 1c). For example, SSAD in phosphate-buffered saline (PBS) or low M_w HAMA solution presented a large aggregation formation, whereas it was evenly dispersed in 1000 kDa of 1 w/v% HAMA. Further investigation was performed using HAMA of 1000 kDa with different concentrations. Out of the tested concentrations, 0.5–1 w/v% HAMA solutions exhibited excellent SSAD distributions, yet small aggregates could still be found in the concentration of 0.25 w/v% (Figure 1d), consequently leading us to apply 0.5 w/v% HAMA in the final formulation. Indeed, as we expected, the zeta potential of SSAD in PBS solution showed a positive value (Figure S1, Supporting Information); in contrast, the zeta potential of the HAMA solution presented a negatively charged surface due to its abundant carboxyl

C. Schuurmans
Department of Pharmaceutics
Utrecht Institute for Pharmaceutical Sciences (UIPS)
Science for Life
Utrecht University
Universiteitsweg 99, 3508, TB, Utrecht, The Netherlands
X. Zhang
John A. Paulson School of Engineering and Applied Sciences
Harvard University
Cambridge, MA 02138, USA
E-mail: xingcai@mit.edu
X. Zhang
School of Engineering
Massachusetts Institute of Technology
Cambridge, MA 02139, USA

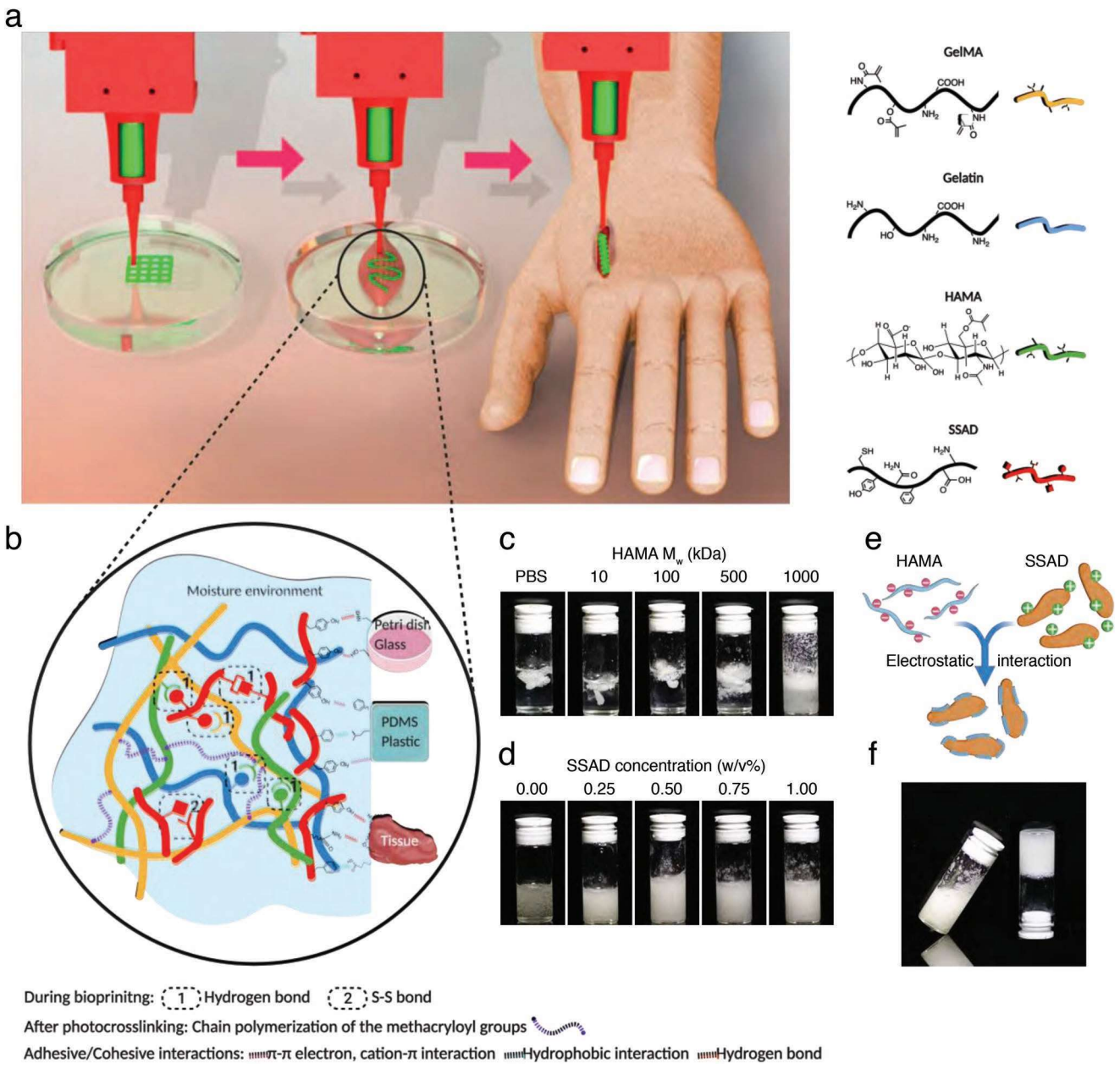

Figure 1. Illustrations of extrusion bioprinting under wet conditions and the composition of the adhesive/cohesive bioink. a) A diagram of the bioprinting process, including bioprinting in wet conditions, testing in vitro, and in situ bioprinting. b) The interactions within the bioink include primarily S—S bond and hydrogen bonds, which contributes to the bioink cohesiveness. The chain polymerization of GelMA and HAMA after photocrosslinking further introduces stable chemical bonds. The adhesive mechanisms include π–π electron, cation–π interaction, hydrophobic interactions, hydrogen bonds, as well as metal coordination bonds between the deposited bioink and different substrates, including tissue culture-treated petri dish, glass, PDMS, plastic (pristine polystyrene), and biological tissues. c) SSAD distribution in HAMA solutions with different M_w under the same concentration (1.0 w/v%). d) SSAD distribution in HAMA (M_w = 1000 kDa) solutions with different SSAD concentrations. e) Schematic showing negatively charged HAMA neutralizing positively charged SSAD through electrostatic interactions. f) Photograph of the selected bioink with well-distributed SSAD.

groups. Once they were contacted via electrostatic interactions, the negatively charged HAMA could cover and neutralize positively charged SSAD, resulting in better suspension stability of the latter (Figure 1e,f, Supporting Information).

To establish a bioink with favorable bioprinting fidelity, GelMA and gelatin were further added to the HAMA/SSAD suspension. GelMA has been widely proven as a bioink with good biocompatibility in supporting cell adhesion and proliferation due to the presence of intrinsic arginine-glycine-aspartic acid (RGD) sequence,[27,28] and it serves as a photocrosslinkable biomaterial for light-based, on-demand crosslinking to enhance structural integrity. Moreover, gelatin was incorporated to the bioink not only to increase the bioink viscosity and temperature sensitivity but also to provide space for cell spreading and migration after its removal from the hydrogel post-bioprinting.[29] As shown in Figure S2, Supporting

Information, the presence of 5 w/v% gelatin could further contribute to the stability of SSAD dispersion when compared to the bioink without gelatin due to the increased viscosity.

To test our bioink components, a series of formulations were assessed for extrusion bioprinting in wet conditions, including GG (GelMA/gelatin, 5/5 w/v%), GGS (GelMA/gelatin/SSAD, 5/5/0.5 w/v%), GGH (GelMA/gelatin/HAMA, 5/5/0.5 w/v%), GHS (GelMA/HAMA/SSAD, 5/0.5/0.5 w/v%), and GGHS (GelMA/gelatin/HAMA/SSAD, 5/5/0.5/0.5 w/v%). The adhesion abilities of hydrogels with different formulations were evaluated using a mechanical tester (**Figure 2**a). We first performed lap-shear studies of different bioink formulations on porcine skin in the non-wetted state. As shown in Figure 2b, the shear adhesion of GGHS could reach 17.0 ± 1.6 kPa, whereas in the group without SSAD or poorly dispersed SSAD exhibited weak adhesions (6.1 ± 2.3, 5.8 ± 1.1, and 9.3 ± 0.6 kPa for GGH, GGS, and GHS, respectively). However, compared with SSAD-alone adhesion as we previously reported,[22] the adhesive strength observed in GGHS was slightly decreased. This result suggested that while HAMA had a positive influence on SSAD distribution, HAMA also partially covered the adhesive motif of SSAD, which resulted in its adhesive strength-reduction. The adhesion strength observed however, was still decently strong compared to most non-designed bioinks for such an application, and was deemed sufficient to achieve stable bioprinting in wet conditions.

Since tissue adhesion is an essential factor for a number of general bioprinting scenarios inclusive of IOB applications, we subsequently assessed the adhesion performances of the adhesive bioink formulations on the tissues with wet conditions (Figure 2c). We observed that the adhesive strength of GGHS was remarkably higher than the other bioink compositions in the presence of moist as well. The quantification data presented that the 0.5 w/v% SSAD-containing GGHS bioink had an adhesive strength of 13.2 ± 1.8 kPa, approximately fourfold higher than that of the control group (GG). The loss of adhesion of GHS was attributed to the decreased SSAD distribution in the absence of gelatin. Figure S2, Supporting Information, reveals the reaggregation of SSAD in the GHS sample after 15 min storage due to less viscosity when compared to GGHS. Moreover, as indicated by the peeling tests shown in Figure 2d, the rhodamine-labeled, red hydrogel residues were apparent on the side of porcine skin in the GGHS group. In contrast, there was rarely any residue found on the surfaces covered by the groups without SSAD after peeling of the hydrogels. Additionally, the adhesive properties of our adhesive bioink (GGHS) with various biological tissues were further evaluated under wet conditions, and the results are shown in Figure 2e and Figure S3, Supporting Information. Biological tissues, including porcine skin, fat, heart, intestine, kidney, and liver with wet surfaces, were evaluated to mimic clinical conditions. The results displayed that the adhesive bioink formulation easily adhered to different tissues, where adhesive strength was highest on the skin and lowest on the liver tissue. The inequalities in the adhesive strengths were mainly caused by the different densities of functional groups presented on the various surfaces of the tissues as well as their deformability. As an enabling bioink, the abundant hydrogen bonds formed among the GelMA, HAMA, SSAD molecules, and relevant bonds within the SSAD, among others, could enhance the physical stability and cohesiveness of the extruded bioink in wet conditions. Moreover, the versatility of interactions of SSAD and other surfaces primarily contributes to the adhesive properties, which rely on the chemical features of substrate surfaces.[20]

The optimization of different bioink formulations was also investigated by characterizing their physical properties, including viscosities, mechanical properties, swelling ratios, and in vitro degradation profiles. As observed in Figure 2f, temperature varied the viscosities of the different bioinks. The apparent viscosity of the bioink without gelatin (GHS) was not noticeably sensitive to temperature. In contrast, the viscosities of bioinks containing gelatin (5 w/v%) decreased over three to four orders of magnitude (from 10^3 pascal-second (Pa s) to 1 Pa s) when increasing the temperature from 15 to 37 °C, resulting from helix-coil transition of gelatin molecules between 28 and 31 °C. The temperature-variant viscosity would favor successful bioink extrusion at mild temperatures (such as 28 °C) and good shape-fixation after extrusion at room temperature. The bioink of GG showed the lowest viscosity at 37 °C. By contrast, the incorporation of SSAD in the bioink (GGS) increased the viscosity due to the reinforcing effect of SSAD. In addition, HAMA could also increase the viscosity of the bioink (GGH) due to potential electrostatic interaction with gelatin. This hypothesis was supported by the obvious aggregation of SSAD in the bioink of GHS (Figure S4a, Supporting Information). Therefore, the presence of gelatin enhanced the dispersion of SSAD in the bioink of GGHS (Figure S2, Supporting Information), which was in good agreement with our previous observation. To facilitate good printability, we set a mild printing temperature of 28 °C. The amplitude-sweep measurements showed that all the inks exhibited a solid-like response, where the plateau storage modulus (G′) exceeded the loss modulus (G″) at low shear stresses, while behaving like a liquid above the yield stress at 28 °C (Figure 2g). In the absence of SSAD, GG showed a very low plateau modulus and low yield stress (<0.1 Pa), which are not favored for high-resolution printing. Compared with other bioinks, GGHS possessed a relatively low yield stress of ≈80 kPa, allowing the bioink to be extruded at a lower pressure. The moderate yield stress of GGHS enabled omnidirectional patterning of the extruded cylindrical filaments for bioprinting of complex structures at a relative mild extrusion stress. At this temperature, the bioink of GGHS showed good printability, as confirmed by the prominent shear-thinning behavior at 28 °C (Figure S4b, Supporting Information).

The compressive modulus assessments illustrated an expected positive correlation with prepolymer concentration of the bioink (Figure 2h). The presence of HAMA and SSAD significantly enhanced the compressive moduli of the resulting constructs, ranging from 27.7 ± 1.4 kPa for GG, 47.2 ± 2.9 kPa for GGH, to 58.6 ± 5.0 kPa for GGHS. In addition, the swelling ratios of the constructs made by different formulations were identified as inverse correlation with prepolymer concentration of the bioink. The results displayed that the swelling ratio dramatically decreased when the bioink was supplemented with HAMA (Figure 2i), while the addition of SSAD showed no significant influence on the swelling behaviors. As a result of the relatively low swelling ratio, the volume changes should be minimal after implantation, which makes it beneficial for future clinical applications as an adhesive bioink. Furthermore, the degradation was faster in GG samples since they contained uncrosslinked gelatin (Figure 2j).

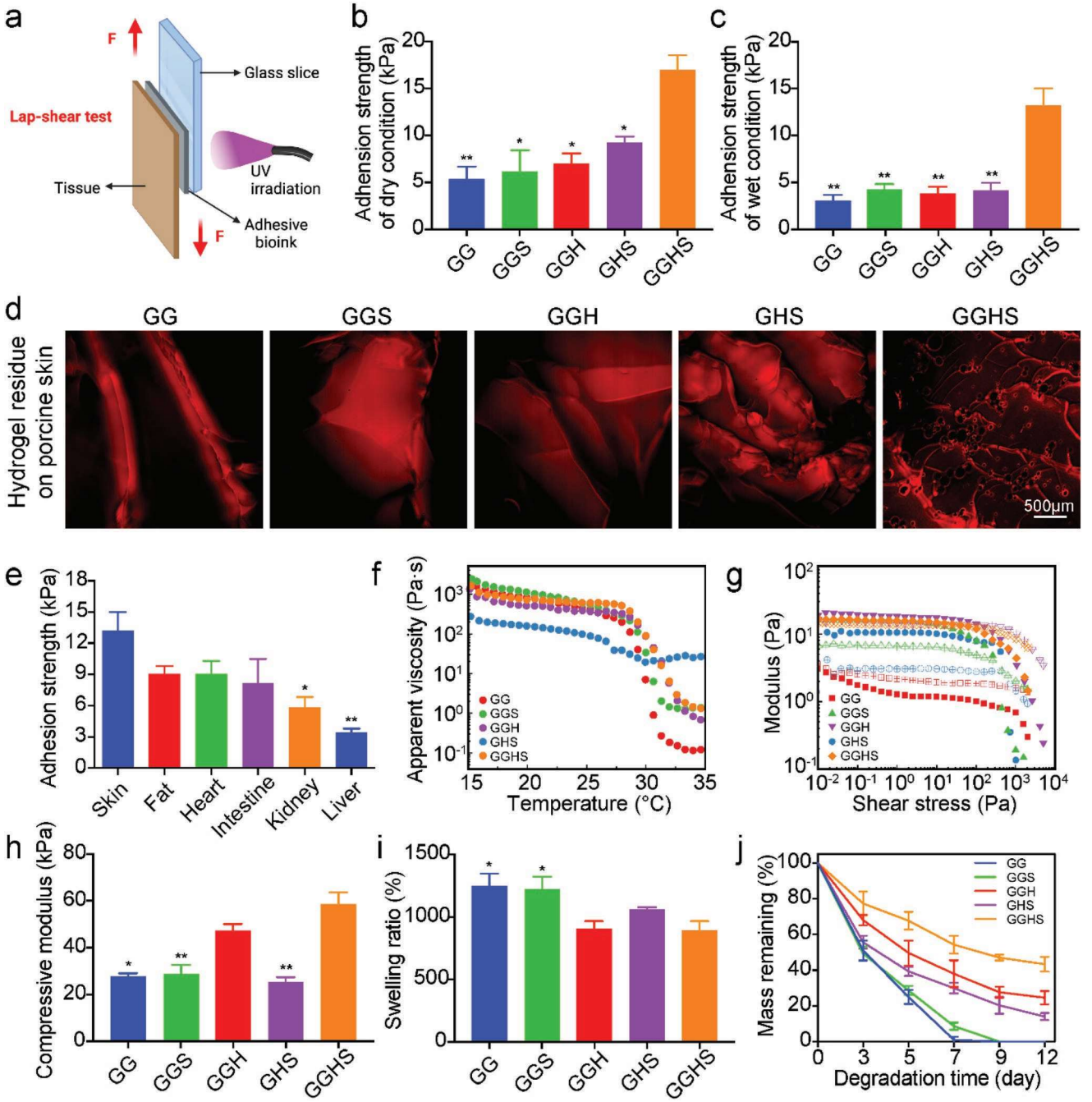

Figure 2. Adhesive properties and physical characterizations of bioinks with different formulations. a) Illustration of the experimental setup for the lap-shear test. b) Adhesion strengths of GG, GGS, GGH, GHS, and GGHS bioinks in dry conditions. c) Adhesion strengths of GG, GGS, GGH, GHS, and GGHS bioinks in wet conditions. d) The hydrogel residues were found on the porcine skin after adhesion-breakage. e) Comparison of adhesive strengths of GGHS hydrogel on different tissues, including porcine skin, fat, heart, intestine, kidney, and liver. f) Apparent viscosities as a function of temperature from 15 to 37 °C for bioinks with different formulations. g) Amplitude sweeps showing shear storage (solid markers) and loss (open markers) moduli as a function of shear stress for bioinks with different formulations at 28 °C. h) The compressive moduli of bioink-formed constructs with different formulations. i) Swelling ratios of bioink-formed constructs with different formulations. j) In vitro degradation profiles of constructs made from bioinks with different formulations. b,c,h, i) $*p < 0.05$, $**p < 0.01$; one-way ANOVA (compared with GGHS group); $n = 3$. e) $*p < 0.05$, $**p < 0.01$; one-way ANOVA (compared with skin group); $n = 3$. j) $*p < 0.05$, $**p < 0.01$, $***p < 0.001$; one-way ANOVA (compared with the day 0 of GGHS group); $n = 3$.

For GGHS samples, the remaining mass was more than 45% at day 12, whereas the same formulation without SSAD had 25% remaining. Therefore, the inclusion of SSAD in the bioinks did bring changes in their degradation profiles. Our results led us to conclude that GGHS proved to be the best bioink formulation among the ones that we tested. Therefore, the final formulation of the adhesive/cohesive bioink was fixed at 5 w/v% GelMA, 5 w/v% gelatin, 0.5 w/v% HAMA, and 0.5 w/v% SSAD.

For extrusion bioprinting, the bioinks are required to allow continuous extrusion and then rapid stabilization to form their intended patterns, which is typically achieved by using biomaterials of high viscosities, with shear-thinning properties, or with stimuli (e.g., temperature) responsiveness.[30–32] Cohesion is another crucial factor that influences the bioink integrity especially during bioprinting in wet conditions. As **Figure 3**a shows, the control bioink consisting of 5 w/v% GelMA and 5 w/v%

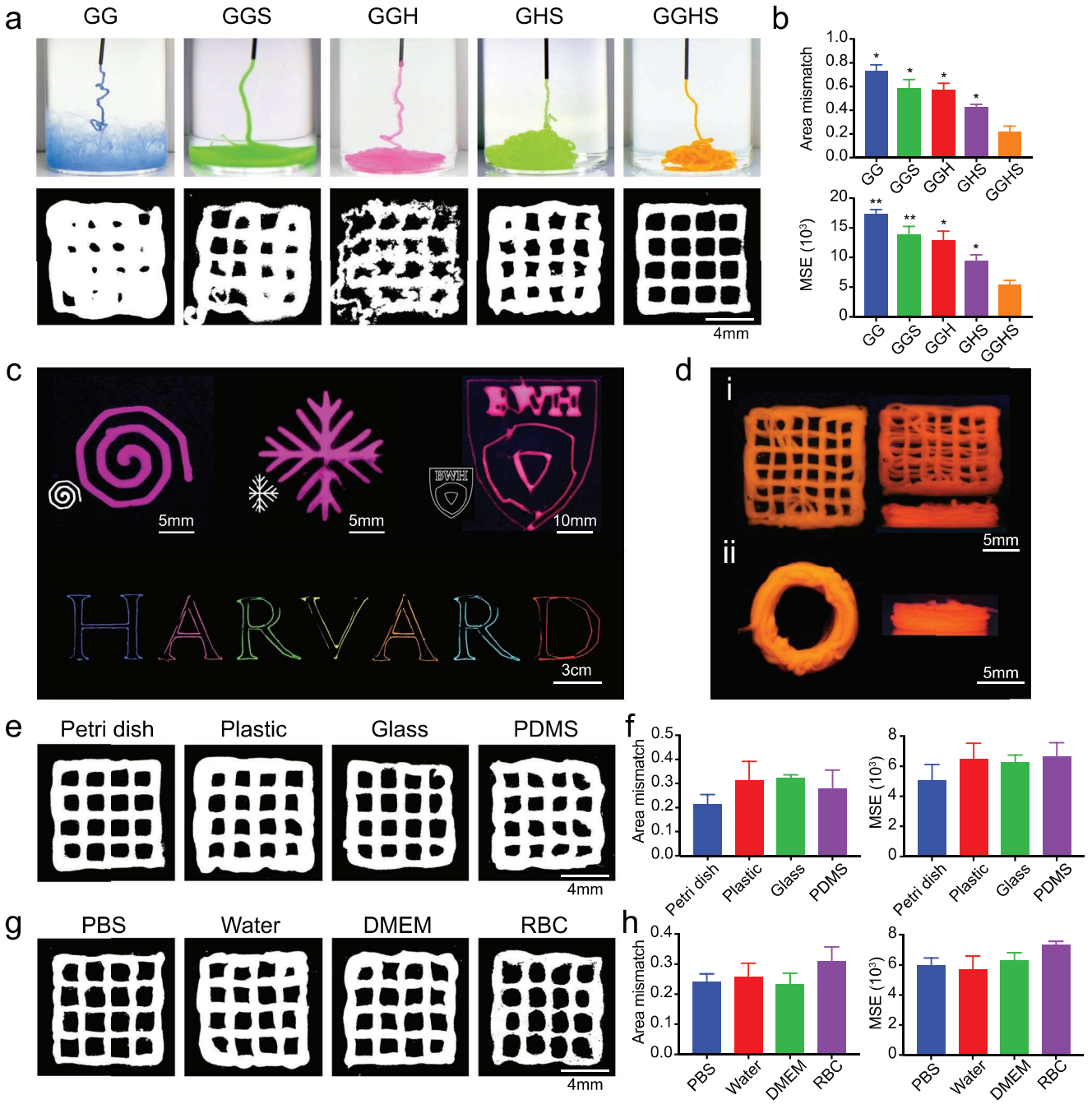

Figure 3. Investigation of printability of different bioink formulations in wet conditions and wet bioprinting with the GGHS bioink. a) Filament morphologies and bioprinted grid structures with the five different bioink formulations in wet conditions on the tissue culture-treated petri dish surface at 25–30 °C. b) Quantitative comparison results of the printed grids and the designed digital pattern. c) Wet bioprinting of complex patterns and multicolor designs onto a tissue culture-treated petri dish at 25–30 °C. d) i) Multi-layer wet bioprinting on the tissue culture-treated petri dish. 0°, 45°, and 90° views of wet-bioprinted grid; ii) 0° and 90° views of wet-bioprinted cylindrical structure with 10 layers. e) Bioprinted grid structures on different substrate surfaces (labeled on the top) in PBS solution. f) Quantitative comparison results of printed grids on different printing surfaces and the designed digital pattern of the grid. g) Bioprinted grid constructs in different solutions (labeled on the top) on tissue culture-treated petri dish surface. h) Quantitative comparison results of printed grids in different solutions and the designed digital pattern of the grid. b) $*p < 0.05$, $**p < 0.01$; one-way ANOVA (compared with GGHS group); $n = 3$.

gelatin (GG) only had weak adhesiveness and supported fiber-formation for a limited time during underwater extrusion, and the cohesiveness was also insufficient leading to rapid disintegration upon vibration. Meanwhile, the addition of SSAD alone (GGS) did not affect the bioink filament formation within water due to the uneven distribution of SSAD in GGS. In comparison, the cohesiveness of the bioink was enhanced in the presence of 0.5% w/v HAMA in GGH attributed to the increased hydrogen bonding, yet the addition of HAMA itself did not affect the bioink adhesiveness. Notably, the well-distributed SSAD in HAMA when both components were present, acted as the main factor in regulating the filament formation and faithful deposition underwater. This result indicated that when supplementing SSAD in HAMA and GelMA/gelatin, electrostatic interactions between the positively charged SSAD and negatively charged HAMA further improved cohesive forces together with the hydrogen bonding formed in this system.

Accordingly, the printing fidelity was assessed by depositing grid patterns of three layers underwater using the five types of bioinks (without subsequent photocrosslinking) at room temperature. The bioprinted structures presented noticeable differences (Figure 3a). The control bioink (GG) showed low adhesion and cohesion when bioprinting underwater, and thus rapidly experienced instability. In contrast, the inclusion of HAMA did not significantly improve the adhesiveness of the bioink during bioprinting of the pattern, although the cohesiveness was satisfactory. The bioink containing HAMA, therefore, achieved fine filaments due to the elevated cohesion but low adhesion during extrusion, resulting in a disordered pattern. Significantly, when all four components (GGHS) were present, optimal underwater bioprinting of a well-defined, multi-layer, highly stable grid structure could be achieved. Quantitative results of area-mismatches and mean squared errors (MSEs) further confirmed the promoted printing fidelity using the GGHS bioink (Figure 3b), which were consistent with qualitative observations from the photographs. It should be noted again that, when bioprinting in the air using the bioink containing 5 w/v% GelMA and 5 w/v% gelatin (GG), the process was smooth (Movie S1, Supporting Information), consistent with what we and others previously demonstrated.[33] The same formulation, unfortunately, could not be bioprinted within the water environment, exhibiting dispersed segments shortly after extrusion leading to the inability to maintain any visible shape upon mechanical disturbance of the surrounding water (Movie S2, Supporting Information). Nevertheless, when applying our GGHS bioink, we successfully bioprinted the structure underwater that intimately attached to the bottom of a tissue culture-treated petri dish along with each adjacent layer in the same construct (Movie S3, Supporting Information). The bioprinted sample maintained the structure even when it was removed from the wet condition (Figure S5 and Movie S4, Supporting Information), indicating that our bioink supported shape fidelity of extruded constructs in the highly variable wound environments in terms of the wet conditions. Meanwhile, Movie S5, Supporting Information, also shows that the bioink formed with GGHS enabled to bioprint same pattern in the air, suggesting its versatility.

Using the selected bioink formulation (GGHS), we then assessed the influence of bioprinting parameters in underwater printing, including interlayer distance, nozzle size, nozzle moving speed, and water temperature, on the bioprinting performances. The bioprinting fidelity was evaluated by comparing the bioprinted structures with the designed digital pattern (Figures S6–S9, Supporting Information).[34] We observed bioprinting disturbance with the distances between the deposited layer and the nozzle tip below 0.05 mm, and bioprinting accuracy was achieved in the distances of 0.075 and 0.2 mm, but mismatches became noticeable after further increasing the distance (Figure S6, Supporting Information). Additionally, the smaller the nozzle size was, the finer filaments and the more precise grid structures were produced (Figure S7, Supporting Information). However, the smallest size of the nozzle (30 gauge (G)) did not necessarily promote the resolution because it could induce continual clogging of the bioink at the tip.[35] Moreover, the nozzle moving speeds between 100 to 400 mm min^{-1} were confirmed to be the proper settings for bioprinting (Figure S8, Supporting Information). As another important factor, water temperature, also affected the bioprinting capacity since GelMA and primarily gelatin, both have thermogelling properties,[36] where either overly low (e.g., 15 °C) or high temperatures (e.g., 55 °C) reduced shape fidelity, and temperatures close to room and body temperatures (25–45 °C) seemed to be optimal (Figure S9, Supporting Information). Understanding the effects of these key bioprinting parameters is essential for applying the cohesive bioink toward bioprinting under wet conditions. Based on the optimized bioprinting conditions, the selected adhesive bioink (GGHS) enabled to bioprint diverse complex constructs on tissue culture-treated petri dish in the water-immersed environment (Figure 3c). Importantly, the bioprinted 3D structures, circle with 10 layers, could resist perturbation even without the need for photocrosslinking. The bioprinted structure disturbed by shaking (200 rpm for 30 min) before UV crosslinking and they kept the same patterns as pre-perturbation. We did not find any significant influence of this level of perturbation on the integrity of the bioprinted structures, as indicated by the quantitative data of MSEs and area-mismatches (Figure S10, Supporting Information).

As discussed, there are diverse possible interactions between the components of our bioink and the different surfaces. We subsequently evaluated the adhesion of the bioprinted scaffolds onto a variety of substrates with dissimilar surface chemical properties, all immersed in an aqueous solution (Figure 3e,f and Figure S11, Supporting Information). Apart from the tissue culture-treated petri dish surfaces, tissue culture-untreated polystyrene plastic, glass, and polydimethylsiloxane (PDMS) served as additional wet bioprinting substrates and presented encouraging adhesion results with the bioprinted patterns. The different interactions as illustrated in Figure 3e included for example, hydrophobic interactions such as $\pi-\pi$ interactions and cation$-\pi$ interactions with hydrophobic surfaces, hydrogen bonds with hydrophilic surfaces, as well as their possible combinations.[37,38] Figure 3g,h and Figure S10, Supporting Information, presented that, the fidelity of bioprinted patterns on the underlying tissue culture-treated petri dish immersed in Dulbecco's modified Eagle medium (DMEM) and water remained unchanged, compared with that in PBS. The bioprinted pattern

in red blood cell (RBC) suspension indicated a slight loss of printing fidelity, which might result from the suspended cells hindered the contact of the bioink with the substrate surface and in between layers.

The balance between bioink printability and biological performance is always a challenge for 3D bioprinting. For instance, the smaller needle size or the lower temperature that benefits the deposition fidelity may lead to cellular damage during the bioprinting process.[39] Considering all the bioprinting parameters that we have already optimized and the cell-friendly settings, needle size of 27G as the nozzle, 200 mm min^{-1} as the nozzle moving velocity, 0.1 mm as the interlayer distance, and 25–30 °C as the medium temperature were determined to be the bioprinting conditions for the cells. A hemolysis test was first performed to evaluate the cytocompatibility of these bioprinted constructs. The photographs in **Figure 4**a presented the apparent difference in color between positive control (0.1 v/v% Triton X-100), negative control (PBS), and five bioink formulations. Contrary to the bright red color in the positive control group, all bioink groups were observed to be near-transparent,

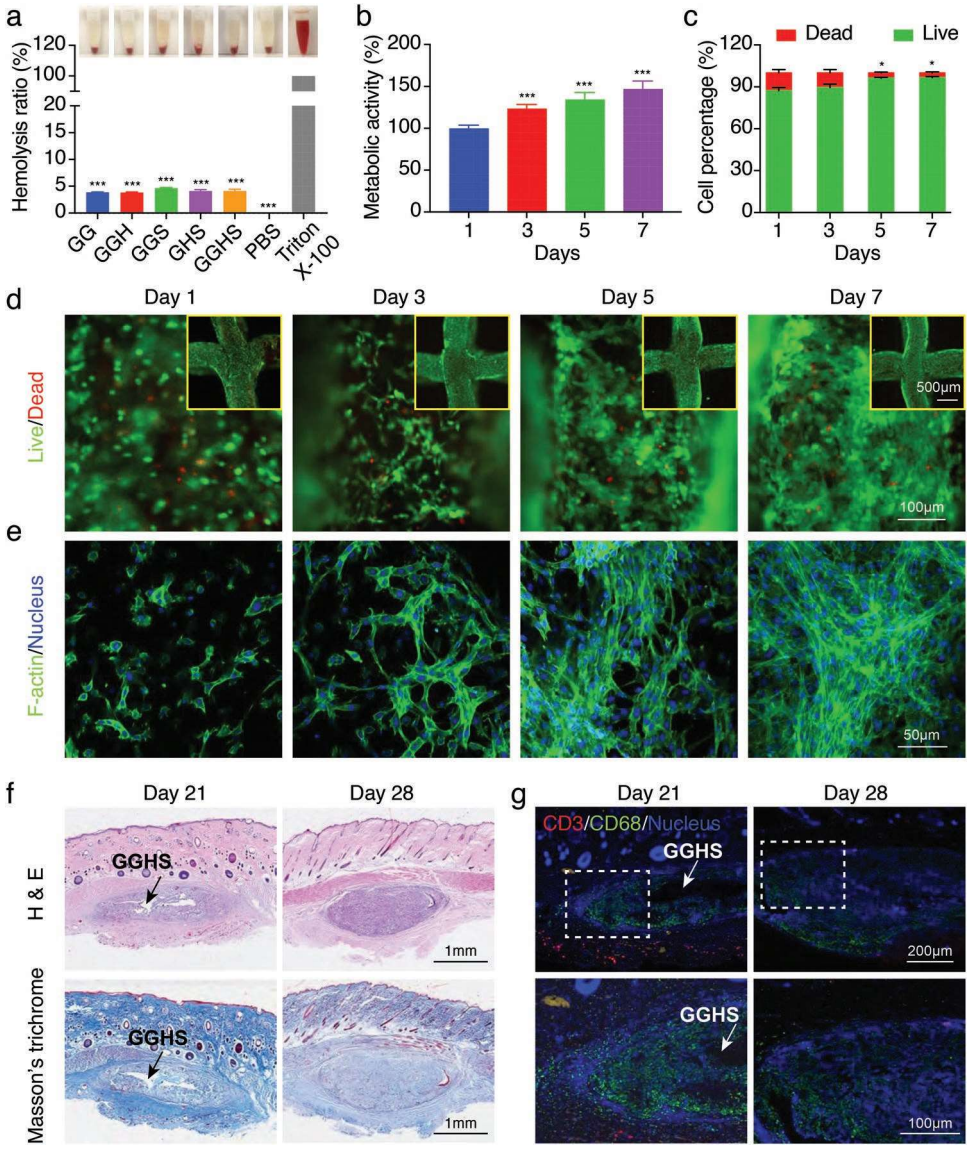

Figure 4. In vitro evaluations of wet bioprinting with the adhesive/cohesive bioink and the in vivo degradation of the GGHS hydrogel. a) Photographs and quantified hemolytic percentages of the constructs made of different bioink formulations. b) The results of MTS assay of NIH/3T3-laden constructs bioprinted with adhesive bioink (GGHS). c) Quantitative results of live/dead staining of NIH/3T3 fibroblasts encapsulated in wet GGHS-bioprinted constructs. d) Fluorescence micrographs of live/dead staining after 1, 3, 5, and 7 days of culture. e) Confocal micrographs showing the F-actin staining results of bioprinted NIH/3T3 fibroblasts in constructs bioprinted with GGHS on days 1, 3, 5, and 7 of culture. f) In vivo degradation of the GGHS hydrogel in the rat subcutaneous implantation model, showing H&E staining and Masson's trichrome staining of the implanted GGHS hydrogel with surrounding tissue at days 21 and 28. g) Immunofluorescence staining of lymphocytes (CD3) and macrophages (CD68) showing immune cell responses around the GGHS-implanted site at days 21 and 28. a) ***$p < 0.001$; one-way ANOVA (compared with Triton-X 100 group); $n = 3$. b,c) *$p < 0.05$, ***$p < 0.001$; one-way ANOVA (compared with day 1); $n = 3$.

similar to the negative control. These consistent results are shown in Figure 4a as the quantitative data, where the constructs formed by our designed bioinks exhibited low hemolysis ratios.

We subsequently conducted bioprinting underwater to further demonstrate the cytocompatibility of our adhesive bioink. NIH/3T3 fibroblasts were encapsulated in the GGHS bioink (5 w/v% GelMA, 5 w/v% gelatin, 0.5 w/v% HAMA, and 0.5 w/v% SSAD) and were bioprinted directly onto the surfaces of the tissue culture-treated polystyrene plastic wells filled with culture medium, followed by UV exposure (10 mW cm^{-2}, 360–480 nm, 30 s). The photocrosslinking after bioprinting is mainly mediated by the radical polymerization of methacryloyl groups in GelMA and HAMA, which provides further structural stability.[40] The bioprinted constructs encapsulated with NIH/3T3 fibroblasts were cultured for 1, 3, 5, and 7 days following bioprinting for live/dead staining and 3-(4,5-dimethylthiazol-2-yl)-5-(3-carboxymethoxyphenyl)-2-(4-sulfophenyl)-2H-tetrazolium (MTS) assay. As shown in Figure 4b, the metabolic activity of NIH/3T3 fibroblasts at day 1 was normalized to 100%, which increased to 123%, 134% at day 3, day 5, and reached close to 150% at day 7, suggesting notable cell growth with culture. Further confirmation with live/dead staining was performed after 1, 3, 5, and 7 days of bioprinting, which implied a highly viable population of the cells (Figure 4c,d, Supporting Information). As also indicated from these images, the bioprinted constructs were stable and maintained their patterns during the culture period. Of note, it was revealed that the cultured NIH/3T3 fibroblasts were homogeneously distributed throughout the bioprinted samples with a spreading morphology (Figure 4d). The shear forces caused by the extrusion of the bioink upon bioprinting might have been the prime reason for the cell death observed on day 1.[33] Furthermore, the results of F-actin staining confirmed that the cells spread extensively after 3 days of bioprinting, with an additional increase in cell density at day 5 and day 7 (Figure 4e). Meanwhile, the fibroblast-like morphology of bioprinted NIH/3T3 showed in the images of F-actin staining was consistent with the normal cell morphology. We also conducted the F-actin staining of NIH/3T3 fibroblasts cast with the same adhesive bioink, exhibiting no deviation of cell morphology when compared to the bioprinted sample (Figure S12, Supporting Information). This remarkable cytocompatibility of the bioprinted constructs should be ascribed to the uncrosslinked gelatin thermally released during the culture period, which provided increased space within the hydrogel networks, resulting in an enhancement of oxygen and nutrient diffusion.

More importantly, hydrogels formed with our GGHS bioink were subcutaneously implanted into Sprague-Dawley (SD) rats under wet conditions to evaluate their degradation in vivo, host immune responses, and interactions with local tissues. The results of hematoxylin and eosin (H&E) staining and Masson's trichrome staining both confirmed the GGHS-based hydrogels sustained a month of time in vivo (Figure 4f and Figure S13, Supporting Information), with the degradation rates of 78.6 ± 2.8% after 21 days and 97.2 ± 0.2% after 28 days, which ensured the healing prior to construct degradation. Additionally, as indicated by the immunostaining results (Figure 4g), the samples induced immune cell infiltration during the 21 day period post-implantation, where a moderate inflammatory response was found in the outermost layers of the implanted hydrogels. After 28 days of implantation, less cellular infiltration was observed from the immunostaining results, indicating the reduced inflammation reaction over time. Overall, these results collectively proved that the adhesive bioink was biocompatible, providing a promising degradable hydrogel platform for wound dressing and tissue repair in vivo.

As a specific example, to extend the application of the designed bioink for IOB in wet conditions, single-channel, and multi-channel handheld extrusion bioprinters were assembled (**Figure 5**a and Figure S13a–c, Supporting Information). Of note, our new multi-channel handheld bioprinter significantly improved upon our previous design,[41] in which it now allowed true ergonomics and full human-directed operations with a built-in push button for extrusion of multiple bioinks with adjustable extrusion nozzles designed for various IOB requirements. With the optimized handheld bioprinting parameters, we successfully produced a collection of sophisticated 2D structures representing lung, heart, intestine, and brain patterns, all underwater on plastic surfaces (Figure 5b). Multi-material bioprinting, which is a fundamental approach for biomimicking tissue heterogeneity, could be combined with our method as well.[42–46] The 3D structures exhibited strong interfacial adhesion between the bioprinted patterns and the substrate (plastic) and between the different layers, facilitating the possibility of hand-writing volumetric constructs with multiple materials (Figure 5c). Notably, the in situ 3D underwater bioprinting with the handheld bioprinter on porcine skin showed strong interfacial adhesion even with stretching, bending, or distorting of the construct-porcine skin combinations (Figure 5d).

Considering various requirements from clinical applications, multiple adaptable nozzles with different designs were subsequently illustrated in this study (Figure 5e). For instance, patients with extensive full-thickness wounds, where dermis and epidermis layers are all damaged, are particularly vulnerable and would take a longer time to heal.[47] One option is the formation of cell-laden tissue constructs with a conformal structure of the wound site. Therefore, we adapted the handheld bioprinter specifically for in situ deposition of skin-precursor sheets with the assistance of our adhesive bioink. Several types of nozzles were designed for full-thickness wound-healing purposes, as schematically shown in Figure 5f and Figure S13d,e, Supporting Information. The design of a separate nozzle was attempted to deposit a stripe-patterned monolayer construct, illustrated by multi-material organization of the sheet with alternating adhesive bioinks in red and green colors. Utilizing the nozzle with different widths of outlets and adjusting the bioink-extrusion speeds, both the volume and the stripe size of bioprinted patterns could be modulated (Figure 5g).

Not only can the adhesive bioinks with different colors share the same bioink composition as proven so far, but they could also differ in their payloads such as cells or growth factors. In our proof-of-concept demonstrations using this multi-nozzle handheld bioprinting method, green fluorescent protein-expressing human umbilical vein endothelial cells (HUVECs-GFP) and red fluorescent protein-expressing HUVECs (HUVECs-RFP) were further bioprinted underwater on tissue culture-treated petri dish. As shown in Figure 5h, the metabolic

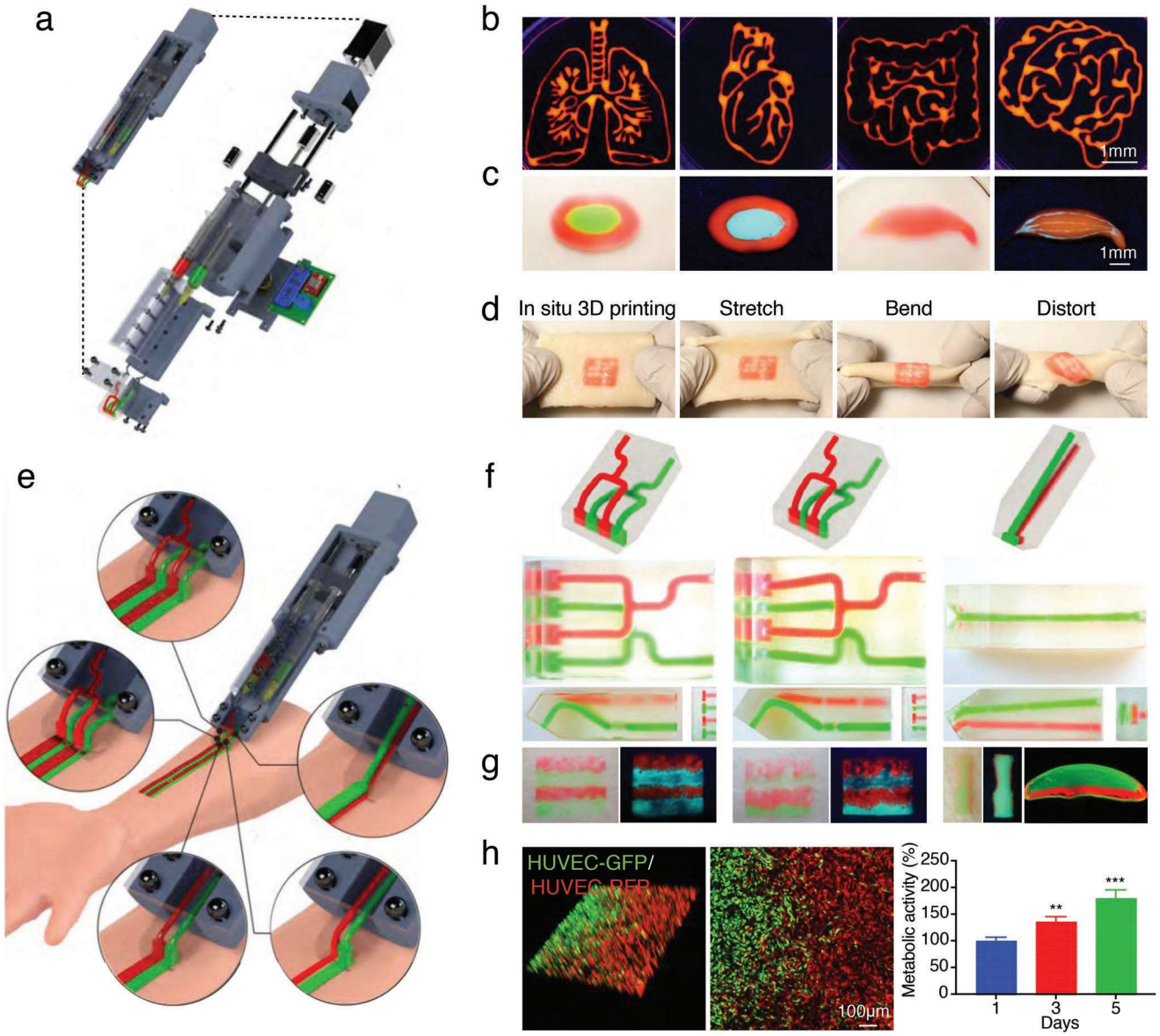

Figure 5. IOB with the handheld extrusion bioprinter. a) Design of the handheld, user-operated, and portable bioprinter. b) 2D hand-written wet bioprinting using the handheld bioprinter on a tissue culture-treated petri dish surface at 25–30 °C. c) 3D patterns bioprinted with the adhesive bioink (GGHS) in wet conditions using the handheld bioprinter on a tissue culture-treated petri dish surface at 25–30 °C. d) Photographs showing in situ bioprinting on ex vivo porcine skin at 25–30 °C. e) Designs of five adjustable nozzles for IOB bioprinting. f) Photographs and designs of the adjustable nozzles. g) Bioprinting patterns with multi-color bioinks using the handheld bioprinter on a tissue culture-treated petri dish surface at 25–30 °C. h) Bioprinted HUVECs using a handheld bioprinter and adjusted nozzle on a tissue culture-treated petri dish surface at 25–30 °C. $^{**}p < 0.01$, $^{***}p < 0.001$; one-way ANOVA (compared with day 1); $n = 3$.

activities of the cells from the MTS assay indicated notable cell proliferation with culture up to 5 days. Further confirmation with fluorescence images suggested excellent cell spreading after 5 days of culture, which implied a highly viable population of the two types of HUVECs. In addition, we performed handheld bioprinting with the multi-layered nozzle, which facilitated the deposition of multiple cell types with control over their thicknesses (Figure S15, Supporting Information). Considering that the skin is composed of two main layers, where the epidermis sits on the top and dermis at the bottom, we attempted to mimic this multi-layer structure by applying this two-layer nozzle with adhesive bioink for bioprinting in wet condition. As a proof-of-concept, a double-layered nozzle enabled the deposition of two different cell types delivered by the adhesive bioink, with HUVECs-GFP on top and HUVECs-RFP at the bottom. As can be seen from Figure S15b, Supporting Information, the results from fluorescence images revealed that HUVECs embedded in the adhesive bioink sheets presented significant spreading, and the MTS assay illustrated cell proliferation (Figure S15c, Supporting Information). Of not, the spatial distributions of the two types of cells could not be entirely maintained as they were designed digitally, due to the cell migration

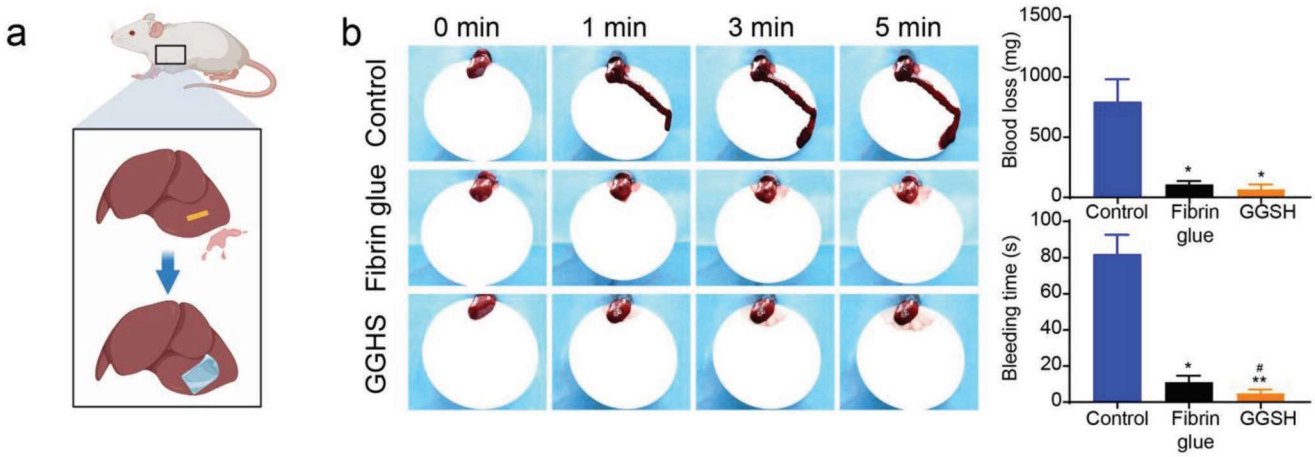

Figure 6. Assessments of hemostatic performance in vivo. a) Schemes of creating the rat liver bleeding model and treating with GGHS bioink or fibrin glue. b) Photographs of liver bleeding at 0, 1, 3, and 5 min, and the quantifications of blood losses and bleeding times. b) $*p < 0.05$, $**p < 0.01$; one-way ANOVA (compared with the control group); $^{\#}p < 0.05$; one-way ANOVA (compared with the fibrin glue group); $n = 3$.

over 5 days of culture. Overall, with the assistance of the adaptable handheld bioprinter build in-house, the excellent adhesion of hand-bioprinted patterns with good cell viability conforming to regular or irregular surface topographies was achieved, demonstrating the potential of direct IOB, which is the key for successful translational applications.

Finally, the bioink formulated by GGHS was utilized for evaluating the in vivo hemostasis performances due to its adhesive properties, good stability, and rapid gelation in wet conditions. **Figure 6**a shows the schematic illustration of the rat liver bleeding model, and the hemostatic process is exhibited in Figure S16, Supporting Information. After puncturing a hole (5 mm in diameter, 3 mm in depth) on the liver, the GGHS hydrogel or fibrin glue was hand-plotted into the hole in wet conditions. The GGHS hydrogel was anticipated to be able to control the extensive bleeding at the wound sites. Indeed, the GGHS group achieved a lower blood loss (69.1 ± 38.2 mg) compared to that with the fibrin glue (108.7 ± 26.5 mg); the control group had the most blood loss, reaching 794.6 ± 187.0 mg (Figure 6b). The bleeding cessation time was 82.0 ± 10.6 s for the blank control group, whereas the hemostasis times of the GGHS bioink and the fibrin glue were 5.0 ± 2.0 s and 11.0 ± 3.6 s, respectively. These results suggested that the GGHS bioink had the desired rapid in vivo hemostatic capacity and could likely protect major wounds during the postoperative healing process.

3. Conclusions

In conclusion, a photocrosslinkable bioink containing a mixture of GelMA, gelatin, HAMA, and SSAD was developed for bioprinting applications, in particular featuring enhanced adhesion in wet conditions. The bioink showed decent adhesion on diverse substrates, including those hydrophilic (glass, tissue culture-treated petri dishes) or hydrophobic (PDMS), and biological tissues, as well as under different aqueous environments, such as water, PBS, cell culture medium, and RBC solution. The bioprinting of planar patterns and volumetric constructs was possible in multi-material and/or multi-layer fashions, where the combination with handheld bioprinters paved a new avenue for in situ bioprinting. Moreover, microfluidic nozzles aided the direct hand-write patterning in wet conditions varying along either the lateral or the vertical direction. In addition, in vivo experiments revealed that GGHS bioink showed favorable hemostasis on liver incision. It should be noted that, the diverse adhesion functions enable, in the future, not only direct IOB on the wet tissue surfaces surrounded by body fluids, but also possibly on pre-existing medical implants that are made of other materials. Taking advantages of the adhesive properties in wet conditions, this adhesive bioink may provide a broad basis for bioprinting in general, as well as utilization as injectable dressings toward applications in regenerative medicine.

Supporting Information

Supporting Information is available from the Wiley Online Library or from the author.

Acknowledgements

W.L., M.W., S.W., and X.W. contributed equally to this work. All animal studies were carried under the approval granted by the Dental School of Chongqing Medical University Animal Care and Use Committee, with the assigned approval number of CQHS-REC-2020-076. The authors gratefully acknowledge funding from the American Heart Association (19TPA34850188) and the Brigham Research Institute. The authors thank the NeuroTechnology Studio at Brigham and Women's Hospital for providing Zeiss LSM880 instrument access and consultation on data acquisition and data analysis. Ximu Z. further acknowledges the program for Youth Innovation in Future Medicine from Chongqing Medical Universtiy (W0075).

Conflict of Interest

Y.S.Z. sits on the scientific advisory board of Allevi by 3D Systems and Xellar, which however, did not participate in or bias the work.

Data Availability Statement

The data that support the findings of this study are available from the corresponding author upon reasonable request.

Keywords

adhesive bioink, bioprinting, Chinese giant salamanders, underwater, wound healing

Received: November 5, 2022
Revised: December 1, 2022
Published online:

[1] N. Ashammakhi, A. Hasan, O. Kaarela, B. Byambaa, A. Sheikhi, A. K. Gaharwar, A. Khademhosseini, *Adv. Healthcare Mater.* **2019**, *8*, 1801048.
[2] A. C. Daly, F. E. Freeman, T. Gonzalez-Fernandez, S. E. Critchley, J. Nulty, D. J. Kelly, *Adv. Healthcare Mater.* **2017**, *6*, 00298.
[3] S. Vijayavenkataraman, W. F. Lu, J. Y. Fuh, *Biofabrication* **2016**, *8*, 032001.
[4] X. Ma, X. Qu, W. Zhu, Y. S. Li, S. Yuan, H. Zhang, J. Liu, P. Wang, C. S. Lai, F. Zanella, G. S. Feng, F. Sheikh, S. Chien, S. Chen, *Proc. Natl. Acad. Sci. U. S. A.* **2016**, *113*, 2206.
[5] S. Knowlton, S. Anand, T. Shah, S. Tasoglu, *Trends Neurosci.* **2018**, *41*, 31.
[6] S. V. Murphy, A. Atala, *Nat. Biotechnol.* **2014**, *32*, 773.
[7] L. Moroni, J. A. Burdick, C. Highley, S. J. Lee, Y. Morimoto, S. Takeuchi, J. J. Yoo, *Nat. Rev. Mater.* **2018**, *3*, 21.
[8] S. Derakhshanfar, R. Mbeleck, K. Xu, X. Zhang, W. Zhong, M. Xing, *Bioact. Mater.* **2018**, *3*, 144.
[9] S. Ahadian, A. Khademhosseini, *Bio-Des. Manuf.* **2018**, *1*, 157.
[10] H. Li, F. Cheng, D. P. Orgill, J. Yao, Y. S. Zhang, *Essays Biochem.* **2021**, *65*, 533.
[11] N. Ashammakhi, S. Ahadian, I. Pountos, S. K. Hu, N. Tellisi, P. Bandaru, S. Ostrovidov, M. R. Dokmeci, A. Khademhosseini, *Biomed. Microdevices* **2019**, *21*, 42.
[12] Y. Wu, D. J. Ravnic, I. T. Ozbolat, *Trends Biotechnol.* **2020**, *38*, 594.
[13] N. Hakimi, R. Cheng, L. Leng, M. Sotoudehfar, P. Q. Ba, N. Bakhtyar, S. Amini-Nik, M. G. Jeschke, A. Günther, *Lab Chip.* **2018**, *18*, 1440.
[14] R. Y. Cheng, G. Eylert, J.-M. Gariepy, S. He, H. Ahmad, Y. Gao, S. Priore, N. Hakimi, M. G. Jeschke, A. J. B. Günther, *Biofabrication* **2020**, *12*, 025002.
[15] C. Di Bella, S. Duchi, C. D. O'Connell, R. Blanchard, C. Augustine, Z. Yue, F. Thompson, C. Richards, S. Beirne, C. Onofrillo, S. H. Bauquier, S. D. Ryan, P. Pivonka, G. G. Wallace, P. F. Choong, *J. Tissue Eng. Regen. Med.* **2018**, *12*, 611.
[16] A. Y. Stark, I. Badge, N. A. Wucinich, T. W. Sullivan, P. H. Niewiarowski, A. Dhinojwala, *Proc. Natl. Acad. Sci. U. S. A.* **2013**, *110*, 6340.
[17] H. Yi, M. Seong, K. Sun, I. Hwang, K. Lee, C. Cha, T. i. Kim, H. E. Jeong, *Adv. Funct. Mater.* **2018**, *28*, 1706498.
[18] L. Heepe, A. E. Kovalev, S. N. Gorb, *Beilstein J. Nanotechnol.* **2014**, *5*, 903.
[19] I. Donderwinkel, J. C. Van Hest, N. R. Cameron, *Polym. Chem.* **2017**, *8*, 4451.
[20] A. H. Hofman, I. A. van Hees, J. Yang, M. Kamperman, *Adv. Mater.* **2018**, *30*, 1704640.
[21] X. Geng, H. Wei, H. Shang, M. Zhou, B. Chen, F. Zhang, X. Zang, P. Li, J. Sun, J. Che, Y. Zhang, C. Xu, *J. Proteomics* **2015**, *119*, 196.
[22] J. Deng, Y. Tang, Q. Zhang, C. Wang, M. Liao, P. Ji, J. Song, G. Luo, L. Chen, X. Ran, *Adv. Funct. Mater.* **2019**, *29*, 1809110.
[23] L. Zheng, Q. Wang, Y. S. Zhang, H. Zhang, Y. Tang, Y. Zhang, W. Zhang, X. Zhang, *Chem. Eng. J.* **2021**, *416*, 129136.
[24] X. Deng, B. Huang, Q. Wang, W. Wu, P. Coates, F. Sefat, C. Lu, W. Zhang, X. Zhang, *ACS Sustainable Chem. Eng.* **2021**, *9*, 3070.
[25] W. Nie, B. Zhang, X. Yan, L. Su, S. Wang, G. Han, D. Han, *J. Nanomater.* **2020**, *2020*, 10848890.
[26] C. Bonnans, J. Chou, Z. Werb, *Nat. Rev. Mol. Cell Biol.* **2014**, *15*, 786.
[27] K. Yue, G. Trujillo-de Santiago, M. M. Alvarez, A. Tamayol, N. Annabi, A. Khademhosseini, *Biomaterials* **2015**, *73*, 254.
[28] G. Ying, N. Jiang, C. Yu, Y. S. Zhang, *Bio-Des. Manuf.* **2018**, *1*, 215.
[29] L. Y. Zhou, J. Fu, Y. He, *Adv. Funct. Mater.* **2020**, *30*, 2000187.
[30] J. H. Chung, S. Naficy, Z. Yue, R. Kapsa, A. Quigley, S. E. Moulton, G. G. Wallace, *Biomater. Sci.* **2013**, *1*, 763.
[31] S. Kyle, Z. M. Jessop, A. Al-Sabah, I. S. Whitaker, *Adv. Healthcare Mater.* **2017**, *6*, 1700264.
[32] Y. S. Zhang, G. Haghiashtiani, T. Hübscher, D. J. Kelly, J. M. Lee, M. Lutolf, M. C. McAlpine, W. Y. Yeong, M. Zenobi-Wong, J. Malda, *Nat. Rev. Methods Primers* **2021**, *1*, 75.
[33] W. Liu, M. A. Heinrich, Y. Zhou, A. Akpek, N. Hu, X. Liu, X. Guan, Z. Zhong, X. Jin, A. Khademhosseini, Y. S. Zhang, *Adv. Healthcare Mater.* **2017**, *6*, 201601451.
[34] J. Gong, C. C. L. Schuurmans, A. M. V. Genderen, X. Cao, W. Li, F. Cheng, J. J. He, A. Lopez, V. Huerta, J. Manriquez, R. Li, H. Li, C. Delavaux, S. Sebastian, P. E. Capendale, H. Wang, J. Xie, M. Yu, R. Masereeuw, T. Vermonden, Y. S. Zhang, *Nat. Commun.* **2020**, *11*, 1267.
[35] K. Kang, L. Hockaday, J. Butcher, *Biofabrication* **2013**, *5*, 035001.
[36] S. Chatterjee, P. C.-l. Hui, C.-w. Kan, *Polymers* **2018**, *10*, 480.
[37] Q. Lu, E. Danner, J. H. Waite, J. N. Israelachvili, H. Zeng, D. S. Hwang, *J. R. Soc. Interface* **2013**, *10*, 20120759.
[38] D. A. Dougherty, *Acc. Chem. Res.* **2013**, *46*, 885.
[39] L. Ning, X. Chen, *Biotechnol. J.* **2017**, *12*, 201600671.
[40] C. Yu, J. Schimelman, P. Wang, K. L. Miller, X. Ma, S. You, J. Guan, B. Sun, W. Zhu, S. Chen, *Chem. Rev.* **2020**, *120*, 10695.
[41] G. Ying, J. Manríquez, D. Wu, J. Zhang, N. Jiang, S. Maharjan, D. H. Medina, Y. Zhang, *Mater. Today Bio* **2020**, *8*, 100074.
[42] R. Singh, R. Kumar, I. Farina, F. Colangelo, L. Feo, F. Fraternali, *Polymers* **2019**, *11*, 62.
[43] J. Visser, B. Peters, T. J. Burger, J. Boomstra, W. J. Dhert, F. P. Melchels, J. Malda, *Biofabrication* **2013**, *5*, 035007.
[44] W. Liu, Y. S. Zhang, M. A. Heinrich, F. De Ferrari, H. L. Jang, S. M. Bakht, M. M. Alvarez, J. Yang, Y. C. Li, G. Trujillo-de Santiago, A. K. Miri, K. Zhu, P. Khoshakhlagh, G. Prakash, H. Cheng, X. Guan, Z. Zhong, J. Ju, G. H. Zhu, X. Jin, S. R. Shin, M. R. Dokmeci, A. Khademhosseini, *Adv. Mater.* **2017**, *29*, 10.
[45] H. Ravanbakhsh, V. Karamzadeh, G. Bao, L. Mongeau, D. Juncker, Y. S. Zhang, *Adv. Mater.* **2021**, *33*, 2104730.
[46] N. Hakimi, R. Cheng, L. Leng, M. Sotoudehfar, P. Q. Ba, N. Bakhtyar, S. Amini-Nik, M. G. Jeschke, A. Gunther, *Lab Chip* **2018**, *18*, 1440.
[47] R. Y. Cheng, G. Eylert, J. M. Gariepy, S. He, H. Ahmad, Y. Gao, S. Priore, N. Hakimi, M. G. Jeschke, A. Gunther, *Biofabrication* **2020**, *12*, 025002.